small
NANO MICRO
www.small-journal.com

Growth of Black Phosphorus Nanobelts and Microbelts

Jun Li, Zhaoshun Gao,* Xiaoxing Ke,* Yangyang Lv, Huili Zhang, Wei Chen, Wanghao Tian, Hancong Sun, Sai Jiang, Xianjing Zhou, Tingting Zuo, Liye Xiao, Manling Sui, Shengfu Tong, Daiming Tang, Bo Da, Kazunari Yamaura, Xuecou Tu, Yun Li, Yi Shi, Jian Chen, Biaobing Jin, Lin Kang, Weiwei Xu, Huabing Wang, and Peiheng Wu*

Black phosphorus nanobelts are fabricated with a one-step solid–liquid–solid reaction method under ambient pressure, where red phosphorus is used as the precursor instead of white phosphorus. The thickness of the as-fabricated nanobelts ranges from micrometers to tens of nanometers as studied by scanning electron microscopy. Energy dispersive X-ray spectroscopy and X-ray diffraction indicate that the nanobelts have the composition and the structure of black phosphorus, transmission electron microscopy reveals a typical layered structure stacked along the *b*-axis, and scanning transmission electron microscopy with energy dispersive X-ray spectroscopy analysis demonstrates the doping of bismuth into the black phosphorus structure. The nanobelt can be directly measured in scanning tunneling microscopy in ambient conditions.

2D materials have tremendous potential for electronic and optoelectronic applications. A good example can be found in graphene due to various novel physical properties.[1–3] However, graphene behaves as metallic or semimetallic due to the absence of bandgap, and thus cannot be used as semiconductor switches in computer circuits. Recently, a new 2D elemental allotrope material, black phosphorus (BP), has attracted increasing attention and is being investigated with lots of efforts.[4] BP has a similarly layered structure, which allows it to be mechanically exfoliated into ultrathin layers of atomic thickness as well.[4–8] More importantly, BP has a direct bandgap in both thin-layer and bulk crystal, and the bandgap varies from ≈0.3 eV for the bulk to 1.5–2.0 eV for monolayer.[4–9] Particularly, the fact that the finite bandgap of BP can be switched between insulating and conducting states as a semiconductor,[8,9] whereas its 2D structure allows fast charge flow in-plane and hence a high mobility, promotes BP promising for electronic applications. On the other hand, the layer structure dependent bandgap covers the entire spectral range from visible to mid-infrared wavelength, which makes BP a promising candidate for the 2D broadband optoelectronic applications.[10–15]

BP has been studied for decades,[12,13] while only from 2014 it was isolated into few layers, i.e., phosphorene, for field effect and optoelectronic devices.[4–7] However, there are still three main challenges for the development of BP.[4–15] First, the synthesis condition is harsh for BP. Although BP can be grown from white or red phosphorus directly, extremely high pressure is necessary.[16,17] For instance, the large single crystalline BP has been fabricated from red phosphorus under high-pressure up to few GPa.[6,18] Alternatively, BP was reported to be grown from red phosphorus under low-pressure with the assistance of

Prof. J. Li, Y. Lv, H. Zhang, W. Chen, W. Tian, H. Sun, S. Jiang, Dr. X. Zhou, Dr. X. Tu, Prof. Y. Li, Prof. Y. Shi, Prof. J. Chen, Prof. B. Jin, Prof. L. Kang, Prof. W. Xu, Prof. H. Wang, Prof. P. Wu
School of Electronic Science and Engineering
Nanjing University
Nanjing 210046, China
E-mail: junli@nju.edu.cn

Prof. Z. Gao, T. Zuo, Prof. L. Xiao
Institute of Electrical Engineering
Chinese Academy of Sciences
Beijing 100190, China
E-mail: gaozs@mail.iee.ac.cn

Prof. Z. Gao, Prof. D. Tang, Dr. B. Da, Prof. K. Yamaura
National Institute for Materials Science
Tsukuba 305-0044, Japan

The ORCID identification number(s) for the author(s) of this article can be found under https://doi.org/10.1002/smll.201702501.

DOI: 10.1002/smll.201702501

Prof. X. Ke, Prof. M. Sui
Institute of Microstructures and Properties of Advanced Materials
Beijing University of Technology
Beijing 100124, China
E-mail: kexiaoxing@bjut.edu.cn

Prof. S. Tong
School of Chemistry
Sun Yat-sen University
Guangzhou 510275, China

Prof. K. Yamaura
Graduate School of Chemical Sciences and Engineering
Hokkaido University
Sapporo 060-0810, Japan

Prof. L. Kang, Prof. P. Wu
Synergetic Innovation Center of Quantum Information and Quantum Physics
University of Science and Technology of China
Hefei, Anhui 230026, China

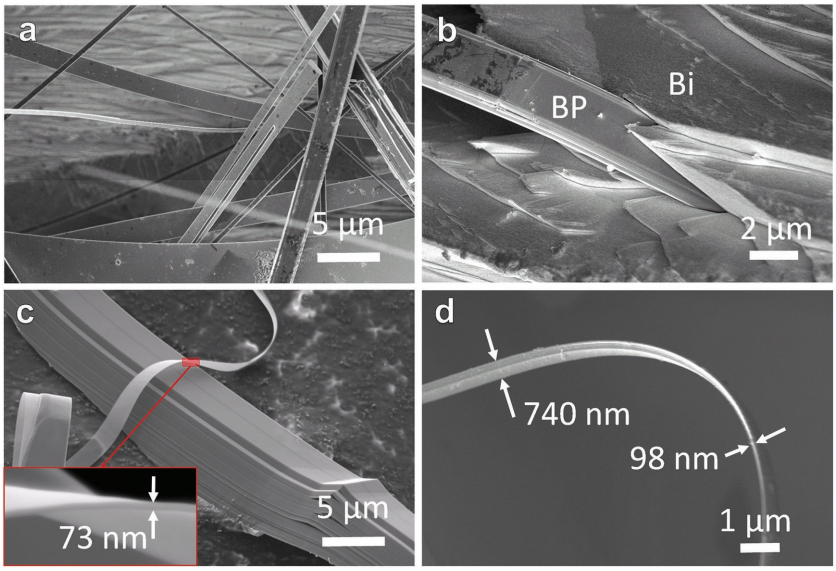

Figure 1. SEM images of BP micro- and nanobelt. a) The size of belts ranges from few micrometers to few hundred nanometers. b) A thick BP belt demonstrates a stack of nanobelts. c) A microbelt as-grown out of the Bi substrate. d) A bended individual bended nanobelt with a width of 740 nm and a thickness of 98 nm.

gold/tin/tin-iodide catalyst.[19] To avoid the external pressure, BP can also be synthesized using mercury or bismuth-flux method from white phosphorus under ambient pressure.[17,20] However, it should be mentioned that the white phosphorus is extremely toxic. Second, the applications of phosphorene in electronics and particularly microelectronics, remain difficult. It is challenging to extract single layers and deposit on substrates, before being patterned for the electronic devices.[1–9] Lastly, BP is well known as an extremely sensitive material to air and moisture, thus it is necessary to use in situ cleaving and surface protection treatment in high vacuum condition,[1–12,21–23] or encapsulation, solvents, molecules, etc.[24–28] In this article, we report on the synthesis and characterization of air-restricted BP nanobelts grown from white phosphorus in ambient pressure.

Figure 1 shows scanning electron microscopy (SEM) images for the BP synthesized on the Bi substrate. The BP show belt-like morphology with high crystallinity. In Figure 1b, a BP belt was observed as grown directly from the bismuth substrate, indicating a possible growth mechanism of epitaxy, which is typical for 1D nanomaterials,[29–32] particularly for the recent report about the catalyst-assisted growth of red phosphorus nanowires.[32] Once visualized from the side, the BP belts show a 2D structure with stacks of ultrathin belts, resulting in a "book-like" structure as shown in Figure 1c. The enlarged view for an individual ultrathin belt (inset of Figure 1c) shows a thickness as low as 73 nm. A bended nanobelt is also given in Figure 1d, and the nanobelt demonstrates good elasticity.

In order to study its initial state for the growth of BP, we synthesized a crystal in quite short time (20 h for cooling) intentionally. As shown in the SEM images of **Figure 2**, short phosphorus nanowires can be found on the surface of the bismuth substrate rather than the micro- or nanobelts as described above. Figure 2a shows an SEM image of a BP nanowire on the Bi substrate, where the distribution of Bi and P was mapped using energy dispersive X-ray spectroscopy (EDX) as shown in Figure 2b,c, respectively. It is interesting to note that the phosphorous nanowire grown out of the bismuth substrate is capped with a bismuth globular-like nanoparticle with comparable diameter to the nanowire. We therefore propose a growth mechanic of the BP nanowire similar to that of carbon nanostructures, where the catalyst-assisted top-growth or bottom-growth of nanostructures is well accepted.[29,30]

X-ray diffraction (XRD) is performed to an individual BP belt for the determination of its structure. We mounted a BP belt onto a glass subtract, and then cleaved the sample into a flat surface with thickness down to around 100 nm. The obtained XRD pattern is shown in **Figure 3**, where a layered structure can be clearly distinguished from the strong peaks at (0 2*n* 0) (*n* is integer), as indexed using the orthorhombic structure of black phosphorous with the space group of *Bmab*(64). The main peak for the rocking curve of (040) shows a narrow full width at half maximum as 0.132° (see right inset of the figure),

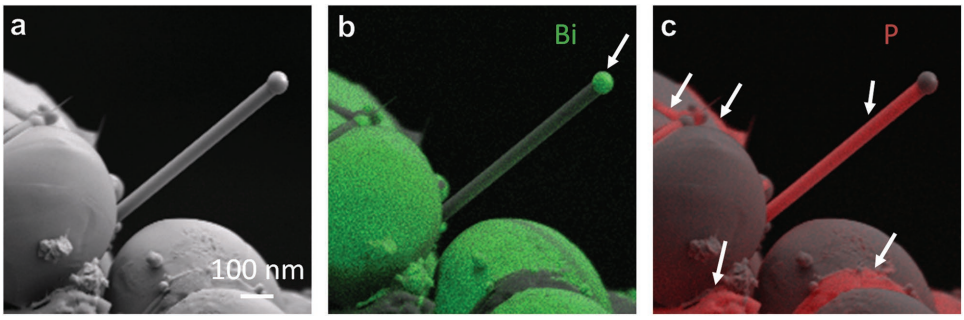

Figure 2. SEM images of BP nanowires at the initial growth stage. a) SEM image of a nanowire-like BP. b,c) Energy dispersive X-ray (EDX) mapping for Bi and P distributions, respectively. Here, the EDX mapping was overlapped onto the SEM image to indicate the distribution of elements referenced to the nanowire and substrate. The capping nanoparticle of Bi is indicated by arrow in (b) whereas the presence of short nanowires is indicated by arrows in (c).

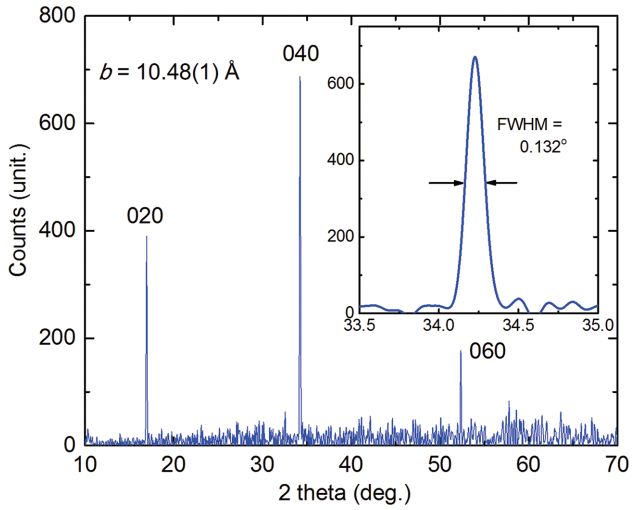

Figure 3. XRD pattern for an individual BP microbelt from the *b*-axis. The left inset is a schematic illustration of the BP lattice viewed along the *c*-axis. The right inset shows the rocking curve of (040) peak, whose full width at half maximum (FWHM) is 0.132°.

suggesting well crystallinity for the nanobelt. This result is consistent with previous results on black phosphorous.[4–7] Moreover, the XRD pattern confirms that the cleavage plane is parallel to the *ac*-plane as illustrated in the schematic drawing of BP lattice shown in the inset of Figure 3. The layer distance along the *b*-axis can be estimated as 10.48(1) Å, being consistent with previous work.[5]

We further conducted structural characterizations on an individual nanobelt using transmission electron microscopy (TEM) (**Figure 4**). Note that an individual nanobelt has a uniform thickness of ≈27 nm (Figure 4a) as shown by bright-field TEM. Figure 4b shows a fast Fourier transform (FFT) pattern corresponding to the red-boxed area on the tip side of the nanobelt as indicated in Figure 4a. The sharp spot perpendicular to the stack direction of the nanobelt can be indexed as (010), corresponding to the layered structure along the *b*-axis. High resolution TEM on the sharp tip demonstrates the single-crystalline layered structure as shown in Figure 4c, where a multilayered structure is clearly observed parallel to the belt axis. Consequently, we can conclude that the growth direction of the belt is along the *ac*-plane, and stacked along [010], namely, the *b*-axis. For accurate elemental analysis on the BP, high angle annular dark field scanning transmission electron microscopy (HAADF-STEM) and EDX were performed using an FEI Titan "cubed" microscope, equipped with an aberration corrector for the probe-forming lens and a Super-X EDX detector, operated at 200 kV. STEM-EDX analysis was carried out on two regions as shown in Figure 4d,e. For the STEM-EDX characterization experiments, the BP belts were first cleaved into nanobelts with thicknesses from 10 to 100 nm, and the as-prepared nanobelts were dispersed in ethanol before being dropped onto a carbon film supported TEM grid. It can be seen that STEM-EDX spectra were taken from two regions of different thickness, where the presence of Bi is confirmed from the spectrum taken from thicker area (region A). Nevertheless, the intensity of Bi is much smaller from the spectrum taken from the thin area (region B), revealing a successful doping of Bi of limited dose in BP.

Temperature dependence of the resistance was measured in Physical Property Measurement System (PPMS-9, Quantum Design Inc.). **Figure 5**a shows the temperature dependence of the resistance (ρ) for an individual nanobelt. The ρ–T curve of the BP nanobelt demonstrates a slightly upturn phenomenon

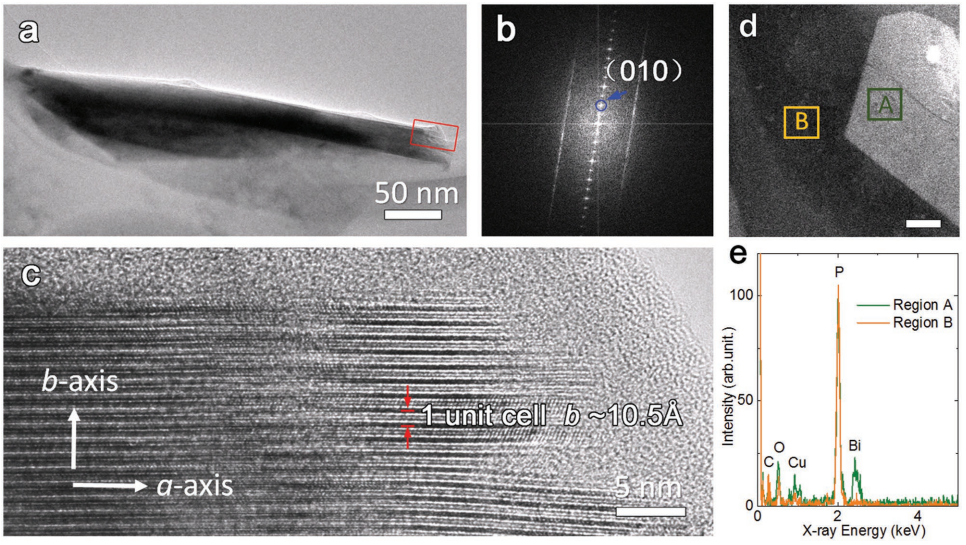

Figure 4. TEM image of a nanobelt. a) An individual nanobelt at low magnification, b) a corresponding FFT pattern where the (010) planes of BP are confirmed, and c) a high resolution TEM image obtained from the boxed area in (a). The layered structure is stacked along [010] direction, i.e., *b*-axis as confirmed from the TEM, and FFT. d) HAADF-STEM image of BP nanosheet at low magnification, and e) STEM-EDX analysis in two regions as indicated in (d). Two regions have a difference in thickness, namely, Region A is thicker (as shown by higher intensity) and Region B is thinner. The presence of Bi is confirmed in EDX spectra, where the thicker region has a higher intensity and the thinner region has a lower intensity.

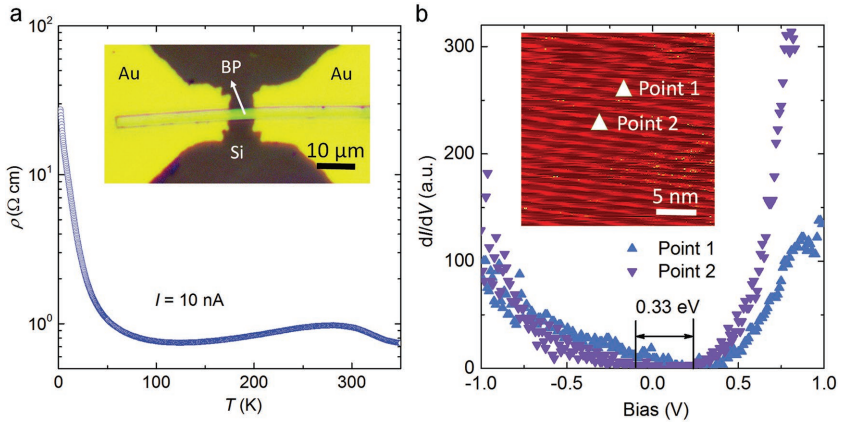

Figure 5. Transport properties of the BP nanobelts. a) Temperature dependence of the resistance for an individual nanobelt (width W = 4.33 μm, h = 50 nm). Inset shows an optical microscopic image of the as-measured sample, where the Au electrodes are patterned using a photolithography and a followed by argon ion etching. b) Two representative tunneling spectra on a BP nanobelt. The bandgap is estimated size of 0.33 eV, being in consistent with the bulk BP crystal (0.30 eV). Inset shows an STM image (V_{bias} = –0.19 V, I_{set} = 1.22 nA) with a scan size of 25 × 25 nm^2.

at the high temperature region above 313 K, following a typical semiconductor behavior at room and low temperatures. The ρ–T curve is similar to those of bulk crystal under hydrostatic pressure of 0.23 GPa, which was applied to suppress the bandgap of the elemental semiconductor.[5] The measurement revealed that the BP nanobelt had a relatively better conductivity than the bulk single crystalline BP synthesized by high-pressure technique.[4–7] It should be emphasized that the ρ of BP decreases with temperatures in the range of 313 to 98 K, exhibiting a metallic-like behavior. We assume that (limited) amount of bismuth or holes have been doped into the lattice of BP, while further studies on the chemical doping are essential to understand the bandgap modification.

We also studied on the nanobelts using scanning tunneling microscopy/spectroscopy (STM/S, MicroNano D-5A, Zhuolun MicroNano Ltd.) to explore the semiconductor bandgap value of the BP. We emphasize that the STM/S measurements are surface-sensitive technique, by which only the topmost surface atomic layer of the materials can be detected, as a result, the STM can probe the local density of states for only a few layer angstroms above the topmost surface. However, the previous BP was generally known as extremely sensitive to air and moisture.[1–9] It is essential to using in situ cleaving and high vacuum conditions for the surface-sensitive measurements.[22,23] Our present STM/S measurements, however, were carried out at ambient condition. Inset of Figure 5b shows a typical STM topographic image of cleaved BP nanobelt with view of 25 × 25 nm^2. Although we can hardly obtain the atomic resolution due to the nonvacuum condition, the observation of STM image on BP indicates the incredible stabilization under oxygen and moisture, which is of greatly important to further researches and applications of BP. Tunneling spectroscopy of three selected points is given in Figure 5b. The spectrums are observed a relatively small semiconductor bandgap value of about 0.33 eV, being slightly less than the bulk crystal (0.30 eV) and also monolayer (2.05 eV). However, it should be mentioned that the bandgap of bulk crystal was measured at low temperature (i.e., 80 K), which could be less than that of room temperature as can be expected from the transport properties.[6]

In summary, single-crystalline BP nanobelts were successfully synthesized using a one-step fabrication method. The nanobelts were observed to have a typical layered structure stacked along the *b*-axis, allowing easy exfoliation into ultrathin layer with the thickness of a few unit cells. We propose a growth mechanism of nanobelts using the catalyst of Bi as similar to that of 1D materials such as carbon nanotubes. The STM/S measurements can be carried out in ambient condition, suggesting the oxygen and moisture restriction properties of BP nanobelts. This facile one-step synthesis technique of air-stable BP has the advantage of eco-friendly where toxic white phosphorus or high-pressure can be avoided, and therefore has a great potential for fabrication at a larger scale.

Experimental Section

Single-crystalline BP was prepared using direct one-step solid–liquid–solid reaction method. The starting materials of powder red phosphorus (3N) and bismuth (5N) were mixed by ball milling for 5 h and placed into an *h*-BN cell. Here, the bismuth was used as flux. The BN cell was put into a stainless steel tube, both ends of which were pressed and sealed by arc welding in an Ar atmosphere. The loaded capsule was heat-treated at 500 °C for 10 h, and then slowly cooled to 250 °C for 45 h. Once heated at 500 °C the superfine red phosphorus can be melted.

Micro- and nanoscaled BP belts were found at the surface and within the bismuth metallic substrate. The BP nanobelts were further mounted onto a high resistance silicon subtract with a layer SiO_2 surface for transport properties measurements. Then, the nanobelts were cleaved and patterned with gold electrodes in an in situ fabrication system for micro- and nanodevies (AdNaNo-Tek Ltd.), where the samples were in inert (Ar) or high-vacuum condition (≈10^{-10} Torr).

Acknowledgements

J.L., Z.G., and X.K. contributed equally to this work. The authors gratefully acknowledge financial support by the National Natural Science Foundation of China (Grant Nos. 11234006, 11227904, 11404016, 61501220, 61521001, 6151101183, 61371036, 61571219, 61574074, 61771234, and 61727805), the National Basic Research Program of China (No. 2014CB339800), Jiangsu Provincial Natural Science Fund (BK20150561 and BK20131032), Opening Project of Wuhan National High Magnetic Field Center (2015KF19), Beijing University of Technology (2015-RD-QB-19), Beijing Nova Program (Z161100004916153), and the Japan Society for the Promotion of Science (JSPS) through a Grant-in-Aid for Scientific Research (15K14133 and 16H04501).

Conflict of Interest

The authors declare no conflict of interest.

Keywords

black phosphorus, nanobelts, STEM, STM

Received: July 20, 2017
Revised: September 28, 2017
Published online: November 24, 2017

[1] A. H. Castro Neto, F. Guinea, N. M. R. Peres, K. S. Novoselov, A. K. Geim, *Rev. Mod. Phys.* **2009**, *81*, 109.
[2] K. S. Novoselov, V. I. Fal'ko, L. Colombo, P. R. Gellert, M. G. Schwab, K. Kim, *Nature* **2012**, *490*, 192.
[3] S. Z. Butler, S. M. Hollen, L. Cao, Y. Cui, J. A. Gupta, H. R. Gutiérrez, T. F. Heinz, S. S. Hong, J. Huang, A. F. Ismach, E. Johnston-Halperin, M. Kuno, V. V. Plashnitsa, R. D. Robinson, R. S. Ruoff, S. Salahuddin, J. Shan, L. Shi, M. G. Spencer, M. Terrones, W. Windl, J. E. Goldberger, *ACS Nano* **2013**, *7*, 2898.
[4] H. Liu, A. T. Neal, Z. Zhu, Z. Luo, X. Xu, D. Tománek, P. D. Ye, *ACS Nano* **2014**, *8*, 4033.
[5] L. Li, Y. Yu, G. J. Ye, Q. Ge, X. Ou, H. Wu, D. Feng, X. H. Chen, Y. Zhang, *Nat. Nanotechnol.* **2014**, *9*, 372.
[6] Z. J. Xiang, G. J. Ye, C. Shang, B. Lei, N. Z. Wang, K. S. Yang, D. Y. Liu, F. B. Meng, X. G. Luo, L. J. Zou, Z. Sun, Y. Zhang, X. H. Chen, *Phys. Rev. Lett.* **2015**, *115*, 186403.
[7] L. Li, F. Yang, G. J. Ye, Z. Zhang, Z. Zhu, W. Lou, X. Zhou, L. Li, K. Watanabe, T. Taniguchi, K. Chang, Y. Wang, X. H. Chen, Y. Zhang, *Nat. Nanotechnol.* **2016**, *11*, 593.
[8] J. Kim, S. S. Baik, S. H. Ryu, Y. Sohn, S. Park, B.-G. Park, J. Denlinger, Y. Yi, H. J. Choi, K. S. Kim, *Science* **2015**, *349*, 723.
[9] B. Deng, V. Tran, Y. Xie, H. Jiang, C. Li, Q. Guo, X. Wang, H. Tian, S. J. Koester, H. Wang, J. J. Cha, Q. Xia, L. Yang, F. Xia, *Nat. Commun.* **2017**, *8*, 14474.
[10] N. Youngblood, C. Chen, S. J. Koester, M. Li, *Nat. Photonics* **2015**, https://doi.org/10.1038/NPHOTON.2015.23.
[11] M. Buscema, D. J. Groenendijk, G. A. Steele, H. S. J. van der Zant, A. Castellanos-Gomez, *Nat. Commun.* **2014**, *5*, 4651.
[12] M. Engel, M. Steiner, P. Avouris, *Nano Lett.* **2014**, *14*, 6414.
[13] T. Low, A. Chaves, J. D. Caldwell, A. Kumar, N. X. Fang, P. Avouris, T. F. Heinz, F. Guinea, L. Martin-Moreno, F. Koppens, *Nat. Mater.* **2017**, *16*, 182.
[14] G. Zhang, S. Huang, A. Chaves, C. Song, V. O. Özçelik, T. Low, H. Yan, *Nat. Commun.* **2017**, *8*, 14071.
[15] M. A. Huber, F. Mooshammer, M. Plankl, L. Viti, F. Sandner, L. Z. Kastner, T. Frank, J. Fabian, M. S. Vitiello, T. L. Cocker, R. Huber, *Nat. Nanotechnol.* **2017**, *12*, 207.
[16] J. C. Jamieson, *Science* **1963**, *139*, 1291.
[17] A. Brown, S. Rundqvist, *Acta Crystallogr.* **1965**, *19*, 684.
[18] H. Liu, Y. Du, Y. Deng, P. D. Ye, *Chem. Soc. Rev.* **2015**, *44*, 2732.
[19] S. Lange, P. Schmidt, T. Nilges, *Inorg. Chem.* **2007**, *46*, 4028.
[20] H. Krebs, H. Weitz, K. H. Z. Worms, *Z. Anorg. Allg. Chem.* **1955**, *280*, 119.
[21] R. A. Doganov, E. C. T. O'Farrell, S. P. Koenig, Y. Yeo, A. Ziletti, A. Carvalho, D. K. Campbell, D. F. Coker, K. Watanabe, T. Taniguchi, A. H. Castro Neto, B. Özyilmaz, *Nat. Commun.* **2015**, *6*, 6647.
[22] J. D. Wood, S. A. Wells, D. Jariwala, K.-S. Chen, E. Cho, V. K. Sangwan, X. Liu, L. J. Lauhon, T. J. Marks, M. C. Hersam, *Nano Lett.* **2014**, *14*, 6964.
[23] L. Liang, J. Wang, W. Lin, B. G. Sumpter, V. Meunier, M. Pan, *Nano Lett.* **2014**, *14*, 6400.
[24] J. D. Wood, S. A. Wells, D. Jariwala, K.-S. Chen, E. Cho, V. K. Sangwan, X. Liu, L. J. Lauhon, T. J. Marks, M. C. Hersam, *Nano Lett.* **2014**, *14*, 6964.
[25] D. Hanlon, C. Backes, E. Doherty, C. S. Cucinotta, N. C. Berner, C. Boland, K. Lee, A. Harvey, P. Lynch, Z. Gholamvand, S. Zhang, K. Wang, G. Moynihan, A. Pokle, Q. M. Ramasse, N. McEvoy, W. J. Blau, J. Wang, G. Abellan, F. Hauke, A. Hirsch, S. Sanvito, D. D. O'Regan, G. S. Duesberg, V. Nicolosi, J. N. Coleman, *Nat. Commun.* **2015**, *6*, 8563.
[26] Y. Subburaj, K. Cosentino, M. Axmann, E. Pedrueza-Villalmanzo, E. Hermann, S. Bleicken, J. Spatz, A. J. García-Sáez, *Nat. Commun.* **2015**, *6*, 6647.
[27] J. Kang, J. D. Wood, S. A. Wells, J.-H. Lee, X. Liu, K.-S. Chen, M. C. Hersam, *ACS Nano* **2015**, *9*, 3596.
[28] G. Abellán, V. Lloret, U. Mundloch, M. Marcia, C. Neiss, A. Görling, M. Varela, F. Hauke, A. Hirsch, *Angew. Chem., Int. Ed.* **2016**, *55*, 14557.
[29] S. Iijima, *Nature* **1991**, *354*, 56.
[30] Y. Wu, P. Yang, *J. Am. Chem. Soc.* **2001**, *123*, 3165.
[31] J. Li, J. Yuan, D. M. Tang, S. B. Zhang, M. Y. Li, Y. F. Guo, Y. Tsujimoto, T. Hatano, S. Arisawa, D. Golberg, H. B. Wang, K. Yamaura, E. Takayama-Muromachi, *J. Am. Chem. Soc.* **2012**, *134*, 4068.
[32] J. B. Smith, D. Hagaman, D. DiGuiseppi, R. Schweitzer-Stenner, H.-F. Ji, *Angew. Chem., Int. Ed.* **2016**, *55*, 11829.